RAA 2018 Vol. **18** No. **7**, 79(10pp) doi: 10.1088/1674–4527/18/7/79

http://www.raa-journal.org *http://iopscience.iop.org/raa*

Research in Astronomy and Astrophysics

B-spline surface fitting and simplified GO/PO analysis of subreflector correction for large Cassegrain antenna distortion compensation

You Ban, Cong-Si Wang, Shu-Fei Feng, Wei Wang and Bao-Yan Duan

Key Laboratory of Electronic Equipment Structure Design, Ministry of Education, School of Electromechanical Engineering, Xidian University, Xi'an 710071, China; *banyou_xd@163.com, congsiwang@163.com, sf_feng@foxmail.com, wwang@xidian.edu.cn, byduan@xidian.edu.cn*

Received 2018 March 9; accepted 2018 April 1

Abstract The main surface of a large Cassegrain antenna consists of a large number of panels. There are inevitably random and systematic errors which will degrade the antenna pattern and limit its applicability when working at high frequencies. Correcting the subreflector surface is difficult to describe by a global expansion effectively with a small amount of data. This paper presents a simple and clear way for correcting the subreflector surface of a large Cassegrain antenna for achieving such compensation. The advantage of the method is that the geometrical optics (GO) analysis is extremely simplified by the concept of equivalent prime-focus paraboloid, and corrected deformations of the subreflector surface are determined by simple formulas which represent the relationship between distortions of the subreflector surface and phase of the main surface current. The final shape of the subreflector surface is represented by a B-spline surface. To obtain a satisfactory antenna pattern with the simplest subreflector surface, the optimal number of B-spline patches are searched by particle swarm optimization (PSO). The shaping process is verified by compensating a 22-m Cassegrain antenna whose main reflector has 96 panels. The results are satisfactory and demonstrate the simplicity and effectiveness of the approach.

Key words: telescopes — reflector antennas — subreflector shaping — compensation

1 INTRODUCTION

Large reflector antennas play an important role in applications like radar, communications and radio astronomy (Baars & Krcher 2018). Especially for space explorations and observational astronomy, radio telescopes with a large aperture, high precision and facilities that operate in multi band are scarce. Some famous large dual-reflector telescopes, such as the Sardinia Radio Telescope (SRT) 64-m (Ambrosini et al. 2013), Effelsberg 100-m (Wielebinski et al. 2011), Green Bank Telescope (GBT) 110-m (Prestage et al. 2009), etc., have been built and have made great contributions. China has constructed some large telescopes to support the related research and is preparing the Qitai Radio Telescope (QTT) (Xu & Wang 2016), which will be the world's largest fully steerable dual-reflector antenna in Qitai, China.

However, an antenna's reflector will be distorted by the effects of the environment and technology, which introduce random errors (Ruze 1966) and systematic errors (Duan & Wang 2009), and these errors tend to degrade the antenna's performance. For a dual-reflector telescope, there are three components which can be corrected to compensate the distortions of the main reflector. First of all, for the main reflector, actuators can be placed on the back of the supporting structure for the main reflector, such as in GBT and SRT. Second, it has been widely suggested to use an array type feed (Rahmat-Samii 1991). However, these two methods are usually costly and complicated in applications. Extra weight will also be included in some applications which will increase the burden to the support structure. The last way aims at changing the subreflector surface to compensate for residual errors arising from distortions in the main reflector, which cannot be compensated by adjusting the position of the subreflector. The method that implements a mechanically deformable subreflector is considered to compensate for astigmatic deformation of the main reflector (von Hoerner & Wong 1979). The other approach uses a deformable flat plate which can be referred to in Imbriale (2001). These two methods are compromised of a number of actuators. With the recent development of microstrip reflectarrays, it is proposed to utilize these subreflectarrays as a subreflector to achieve such compensation (Xu et al. 2009) which can be implemented in narrow-band operation. The most simple and effective way is shaping a suitable subreflector surface to achieve compensation. Geometrical optics (GO)/physical optics (PO) and PO/PO analysis methods have been used respectively in Hoferer & Rahmat-Samii (2002) and Gonzalez-Valdes et al. (2013) to calculate the shape of the subreflector surface, and the global Fourier-Jacobi expansions which are related to Zernike polynomials describing the shape of the surface are employed. Actually, a large antenna needs to work at high frequencies and its surface is composed of a large number of panels, so the PO/PO analysis was not able to be realized and the global surface expansions cannot effectively represent the local characteristics of distorted panels with a small amount of data.

In this paper, a simple and efficient approach to correcting the subreflector surface, whose deviation is designed from a perfect hyperboloid, is presented to compensate for the residual error which is the distortion between the real primary surface and its homologous surface. A B-spline surface fitting with particle swarm optimization (PSO) is used to describe the corrected surface. The main part of the method includes two aspects. One is the GO analysis which is simplified by the concept of an equivalent prime-focus paraboloid and deformations of the corrected subreflector surface are determined by their effect on the antenna pattern. The formulas are presented in Section 2. The other one is that the corrected deformations of the subreflector surface are described by a uniform bicubic B-spline surface. The interpolated surface is determined by a small number of control points. PSO has been used to optimize a nonlinear function which represents the relation between an integer number of B-spline patches and the far field pattern. The formulations of the B-spline surface and PSO are presented in Section 3. Section 4 includes an example applying the method in a 22-m Cassegrain antenna whose surface is made up of 96 panels, and the results are satisfactory. Section 5 provides the concluding remarks of the paper.

2 GO/PO ANALYSIS

2.1 PO Analysis for the Far Field Pattern

The telescope's reflector can be treated as a perfect electrical conductor. With the observation point, whose direction is (θ, ϕ), the unit vector is $\hat{\boldsymbol{r}}$ in the far field region, and $\boldsymbol{r}'$ is a point on the reflector surface. The far-field patterns can be calculated by the main reflector PO currents (Rahmat-Samii 1984)

$$\boldsymbol{E}^{\rm PO}\left(\theta,\phi\right) = -jk\eta\frac{e^{-jkr}}{4\pi r}\left(\bar{\bar{\boldsymbol{I}}} - \hat{\boldsymbol{r}}\hat{\boldsymbol{r}}\right) \cdot \int_S \boldsymbol{J}^{\rm PO}\left(\boldsymbol{r}'\right)e^{jk\hat{\boldsymbol{r}}\cdot\boldsymbol{r}'}ds\,, \tag{1}$$

$$\boldsymbol{J}^{\rm PO}\left(\boldsymbol{r}'\right) = 2\hat{\boldsymbol{n}}_{\rm m} \times \boldsymbol{H}^{\rm GO}\,, \tag{2}$$

where j is the unit of the imaginary number, k is the wave number, η is the free-space wave impedance, and $\bar{\bar{\boldsymbol{I}}}$ and $\hat{\boldsymbol{r}}\hat{\boldsymbol{r}}$ are the dyadic of the unit and $\hat{\boldsymbol{r}}$ respectively. S is the reflector surface, $\boldsymbol{J}^{\rm PO}$ is the induced current, $\hat{\boldsymbol{n}}_{\rm m}$ is the unit normal vector on the main reflector surface and $\boldsymbol{H}^{\rm GO}$ is the incident magnetic field which is reflected off of the subreflector.

2.2 GO Analysis with Simplification

The magnetic field of the main reflector can be obtained by GO analysis. Especially for Cassegrain and Gregorian antennas, the concept of an equivalent prime-focus paraboloid (Huang & Jin 1986) is an extreme simplification for GO analysis because it has the same field amplitude and homogeneous phase in the aperture. As shown in Figure 1, the light propagates along a straight line in a homogeneous medium based on Fermat's principle (Silver 1949). According to the principle of energy conservation in a radial pipe, the Cassegrain type design has

$$\left|\boldsymbol{H}^{\rm GO}\right|^2\rho^2\sin\theta_1 d\theta_1 d\phi_1 = \left|\boldsymbol{H}^{\rm GO'}\right|^2{\rho_{\rm e}}^2\sin\theta_2 d\theta_2 d\phi_2\,, \tag{3}$$

where the plane ϕ is perpendicular to the plane θ, and

$$d\phi_2 = d\phi_1\,, \tag{4}$$

$$dS = {\rho_{\rm e}}^2\sin\theta_2 d\theta_2 d\phi_2 = \rho^2\sin\theta_1 d\theta_1 d\phi_1\,. \tag{5}$$

Substituting Equations (4) and (5) into Equation (3) yields

$$\left|\boldsymbol{H}^{\rm GO}\right| = \left|\boldsymbol{H}^{\rm GO'}\right|\,, \tag{6}$$

and there are some relations that

$$\rho = \frac{2F}{1+\cos\theta_1}\,, \tag{7}$$

$$\rho_{\rm e} = M\rho\,, \tag{8}$$

where M is the magnification factor. If e is the eccentricity of the hyperboloid, there is

$$M = \frac{\tan\frac{\theta_1}{2}}{\tan\frac{\theta_2}{2}} = \frac{e+1}{e-1}\,. \tag{9}$$

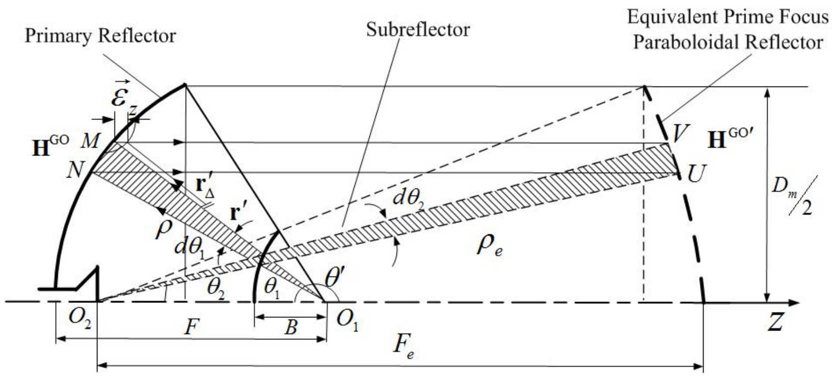

Fig. 1 Equivalent prime-focus paraboloid.

Synthesizing Equations (7) $\sim$ (9), the incident magnetic field $\boldsymbol{H}^{\mathrm{GO}'}$ can be easily obtained because the equivalent prime-focus paraboloid is illuminated by the feed directly. Namely, using a virtual parabola, the complicated Cassegrain antenna is simplified to a single surface antenna with the same feed and aperture, but the equivalent focal length F_{e} is M times the original one (Huang & Jin 1986). This method avoids calculation of the principal radii of curvature such that the ray is reflected off of the subreflector and incident on the main reflector, which makes the calculation simple and fast.

2.3 Deformations of the Shaped Subreflector

In fact, the primary surface of any reasonable antenna will have small errors, and the real surface differs very little from the original one, so the surface normal vector and field amplitude will not deviate substantially compared with an undistorted antenna (Smith & Bastian 1997). If the vector located on the integration points of the distorted reflector is $\boldsymbol{r}'_\Delta$ (see Fig.1), it differs from the corresponding point on the desired undistorted reflector by

$$\boldsymbol{\varepsilon}_z = f_\Delta\left(\boldsymbol{r}'\right)\hat{z}\,, \tag{10}$$

where f_Δ is the scalar value at the integration points defined by $\boldsymbol{r}'$. Then, the integrand in Equation (1) will be multiplied by $e^{jkf_\Delta(\boldsymbol{r}')(\cos\theta-\cos\theta')}$ to calculate the real far field where θ' is the intersection angle between $\boldsymbol{r}'$ and $\hat{z}$. Namely, the main surface distortion will change the path length of the PO currents as

$$\delta_{\mathrm{main}} = f_\Delta\left(\boldsymbol{r}'\right)\left(\cos\theta_1-\cos\theta'\right)\,. \tag{11}$$

There are simple formulas (Ruze 1969) for the phase variation and error of the main reflector surface distortion, axial and lateral feed displacements with similar displacements and rotation of the subreflector. These formulas are verified by the ray tracing method in Mathcad (Lamb & OVRO 2001). Based on these simple formulas, the peak gain of the Cassegrain antenna can be obtained with the subreflector position adjustment and the relationship between the surface accuracy and beam position of the Cassegrain antennas is presented in Zarghamee (1982); and optimal surface adjustment and upgrade of the Haystack antenna (Zarghamee et al. 1995) have received useful guidance. Through the above-mentioned cases, it seems natural to use these simple formulas to determine the deformations of the subreflector surface and compensate. The following formula represents the relationship between subreflector distortions and phase variation of the surface current.

The expression for the change in radio frequency (RF) path length due to distortions in the subreflector surface can be written as

$$\delta_{\mathrm{sub}} = \boldsymbol{a_s}\cdot\boldsymbol{d_s}\,, \tag{12}$$

where $\boldsymbol{d_s} = (d_{s-x}, d_{s-y}, d_{s-z})$ is the displacement of the subreflector surface point. For a paraboloid with the form $z = r^2/(4F)$, the coefficient vector $\boldsymbol{a_s}$ can be expressed as

$$\boldsymbol{a_s} = -\left(\boldsymbol{a_p}+\boldsymbol{a_f}\right)\,. \tag{13}$$

For a Cassegrain antenna (Zarghamee 1982), $\boldsymbol{a_p} = [a_{p-x}, a_{p-y}, a_{p-z}]$ and $\boldsymbol{a_f} = [a_{f-x}, a_{f-y}, a_{f-z}]$, and

$$a_{p-x} = c_p\cos\phi_1\,, \tag{14a}$$

$$a_{p-y} = c_p\sin\phi_1\,, \tag{14b}$$

$$a_{p-z} = -\frac{8F^2}{4F^2+r^2}\,, \tag{14c}$$

$$a_{f-x} = c_f\cos\phi_1\,, \tag{15a}$$

$$a_{f-y} = c_f\sin\phi_1\,, \tag{15b}$$

$$a_{f-z} = -\frac{-4(MF)^2+r^2}{4(MF)^2+r^2}\,. \tag{15c}$$

In addition

$$c_p = \frac{4Fr}{4F^2+r^2}\,, \tag{16a}$$

$$c_F = \frac{4\,(MF)\,r}{4(MF)^2 + r^2}\,. \tag{16b}$$

According to the above mentioned formulas (12) $\sim$ (16), changes in the RF path length which are caused by deformations in the subreflector surface are computed. It can be translated into the antenna phase error by multiplying by k. The whole path length error, which is caused by the main reflector and subreflector, is

$$\delta_{\mathrm{whole}} = \delta_{\mathrm{main}} + \delta_{\mathrm{sub}}\,. \tag{17}$$

In order to recover the far field pattern, the path length error δ_{whole} is expected to be zero. So, the data $\boldsymbol{d_s}$ from the subreflector can be calculated by Equation (17) with the least squares method and then be used to determine functions that can describe the shape of the surface. The variables describing the subreflector surface deformations and optimal method are provided in Section 4.

2.4 Constraints on the Corrected Subreflector

Section 2.3 shows a simplification of the GO analysis in the case of the Cassegrain design. The rays, being from the far field and reflected by the main reflector, must not cross each other before reaching the subreflector when they illuminate the subreflector.

The following states are confined to the primary reflector in a Cassegrain type design with deviations Δz_m. We consider that the deviations have a large positive curvature but a small slope. The reflected rays will cross each other at the critical distance F_c as (von Hoerner 1976)

$$1/F_c = 1/F + 2\Delta z''_m\,, \tag{18}$$

where F is the focal length of an ideal parabolic telescope, and $\Delta z''_m$ is the second derivative in that direction which is the largest.

To derive the subreflector surface that does not have crossing rays, the following formula must be applied (see Fig. 1)

$$F_c \geq F - B\,. \tag{19}$$

Substituting Equation (19) into Equation (18), the general condition is

$$\Delta z''_m \leq \frac{B}{2F\,(F - B)}\,. \tag{20}$$

This section, which provides the limit for correcting a subreflector to compensate for the main surface deviations, is also suitable for other dual-reflector antenna types according to the demand for equal path length (von Hoerner 1976). For example, this is true in the case of Gregorian-type antennas whose incoming rays must have crossed each other before reaching the subreflector.

3 GLOBAL BICUBIC B-SPLINE SURFACE WITH PARTICLE SWARM OPTIMIZATION

To describe the corrected deformations of the subreflector surface, some requirements need to be taken into account for the whole compensatory process (Duan & Rahmat-Samii 1995). Namely, the results can converge easily, the surface can be analytically smoothed through second derivatives and the method can be readily used as a synthesis tool with optimization techniques, so global surface expansions are usually considered. Several functions are evaluated, such as Fourier-Bessel functions, modified Jacobi polynomials and Zernike polynomials. It deserves to be mentioned that modified Jacobi polynomials, which are used in Hoferer & Rahmat-Samii (2002) and Gonzalez-Valdes et al. (2013), are related to Zernike polynomials, and they are different in the index schemes in addition to the normalization constant (Duan & Rahmat-Samii 1995). Actually, optical devices are more precise than microwave antennas, and Zernike polynomials, whose polynomials have a special meaning, have been previously studied and widely applied in the classification of optical aberrations (Doyle et al. 2002). The distortions of examples in Hoferer & Rahmat-Samii (2002) and Gonzalez-Valdes et al. (2013) are also some of the terms in Zernike polynomials, and are well compensated by the shape of the subreflector through their method. However, it is difficult for these global expansions to accurately represent local characteristics with a small number of coefficients, because large antennas are composed of many panels and these panels have diverse local characteristics. There is a statement about this in Section 4.

3.1 B-spline Surface

Based on the above requirements, the surface fitting method of a uniform bicubic B-spline surface (Chiu 1996) is considered. The method is part of the subject of Computer Aided Geometric Design (Farin 2002) and it satisfies the above mentioned requirements, and its other advantages are also obvious. For example, it can accurately represent local characteristics, needs a small amount of data, can be computed and programmed easily, etc. Therefore, the method replaces the global surface expansion to describe the deformation in a subreflector surface. It should be noted that the paper calls a uniform bicubic B-spline surface, which is a type of B-spline rectangular patch defined in spherical coordinates, a B-spline surface.

A B-spline rectangular patch is defined by control points b_{ij} (See Fig. 2), knot vectors $\boldsymbol{U}$ and $\boldsymbol{W}$, and B-

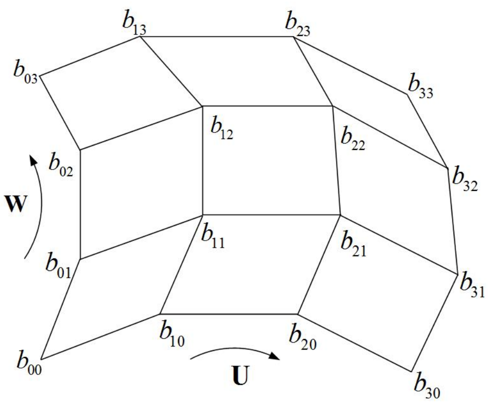

Fig. 2 Bicubic B-spline surface patch.

spline basis functions. The general formula is

$$\begin{aligned} p(u,w) &= \sum_{i=0}^{3}\sum_{j=0}^{3} F_{i,3}(u)\,F_{j,3}(w) b_{ij} \\ &= [U]\,[M_B]\,[b]\,[M_B]^{\mathrm{T}}[W]^{\mathrm{T}} \\ & u,w \in [0,1]\ , \end{aligned} \tag{21}$$

where

$$F_{l,n}(t) = \frac{1}{n!}\sum_{j=0}^{n-l}(-1)^j \frac{n!}{j!\,(n-j)!}\,(t+n-l-j) \qquad l=0,1,\ldots,n\,, \tag{22}$$

$$[U] = \begin{bmatrix} u^3 & u^2 & u & 1 \end{bmatrix}\ , \tag{23}$$

$$[W] = \begin{bmatrix} w^3 & w^2 & w & 1 \end{bmatrix}\ , \tag{24}$$

$$[M_B] = \frac{1}{6}\begin{bmatrix} -1 & 3 & -3 & 1 \\ 3 & -6 & 3 & 0 \\ -3 & 0 & 3 & 0 \\ 1 & 4 & 1 & 0 \end{bmatrix}\ , \tag{25}$$

$$[b] = \begin{bmatrix} b_{00} & b_{01} & b_{02} & b_{03} \\ b_{10} & b_{11} & b_{12} & b_{13} \\ b_{20} & b_{21} & b_{22} & b_{23} \\ b_{30} & b_{31} & b_{32} & b_{33} \end{bmatrix}\ . \tag{26}$$

The B-spline surface is made up of a series of B-spline patches. Two key properties of the method are local modification and second derivatives of the surface. These properties are what the surface expansions really need. Once the characteristic grid vertices b_{ij} are obtained, the global surface can be spliced by the patches.

3.2 PSO for the Number of B-spline Patches

Actually, the data points p can be computed by GO/PO analysis, and the knot vectors $\boldsymbol{U}$ and $\boldsymbol{W}$ are variables determined by PSO. However, the control points b_{ij} need to be computed, so there is a reverse computation of the B-spline surface, and the solution uses the two-way curve method. If the data points p are known, the reverse steps are presented as follows:

(1) Provide the data p_{ij} $(i=1,2,\ldots,m; j=1,2,\ldots,n)$;

(2) Calculate the n characteristic polygons of the n B-spline curves along vector $\boldsymbol{U}$ with the inverse algorithm of B-spline curves as

$$b_{i-1} + 4b_i + b_{i+1} = 6p_i\,(i=1,2,\ldots,m)\ . \tag{27}$$

Add two supplementary equations according to the boundary condition. Take the vertices of the obtained characteristic polygons as $V_{ij}\,(i=0,1,2,\ldots,m+1)$;

(3) Take V_{ij} as the data points and calculate the $m+2$ characteristic polygons in step (2) along vector $\boldsymbol{W}$. Then, the control points b_{ij} are obtained.

The above mentioned steps show how the global B-spline surface is generated. However, the optimal data points p_{ij} are difficult to find as there is a nonlinear relationship between it and the far field pattern. Therefore, the paper uses the PSO method (Robinson & Rahmat-Samii 2004) for global optimization to determine the optimal number m and n of data points p_{ij}.

The following summarizes the PSO. Assume there is a D dimensional search space, and the population

$$X = (X_1, X_2, \ldots, X_{N_u})$$

consists of N_u particles, where particle i corresponds to a D dimensional vector $X_i = (x_{i1}, x_{i2}, \ldots, x_{iD})^{\mathrm{T}}$ which represents the position in the search space and a potential solution. According to the objective function, the fitness of every particle can be computed. The velocity of particle i is $V_i = (V_{i1}, V_{i2}, \ldots, V_{iD})^{\mathrm{T}}$, the individual best fitness is $P_i = (P_{i1}, P_{i2}, \ldots, P_{iD})^{\mathrm{T}}$ and the global best fitness is $P_g = (P_{g1}, P_{g2}, \ldots, P_{gD})^{\mathrm{T}}$. The particles will update their individual velocity and position through individual and global best fitness as

$$V_{id}^{ge+1} = \omega V_{id}^{ge} + c_1 r_1\,(P_{id}^{ge} - X_{id}^{ge}) + c_2 r_2\left(P_{gd}^{ge} - X_{id}^{ge}\right)\ . \tag{28}$$

$$X_{id}^{ge+1} = X_{id}^{ge} + V_{id}^{ge+1}\ , \tag{29}$$

where ω is the weighting factor, $d = 1,2,\ldots,D$, $i = 1,2,\ldots,n$, ge represents the current iterations, and c_1 and c_2 are nonnegative constants that are called scaling factors. r_1 and r_2 are random numbers distributed in $[0,1]$. The detailed algorithms of PSO can be found in

Robinson & Rahmat-Samii (2004). To prevent the particles from searching aimlessly, the position and velocity should be limited to a certain range which is presented in the examples in Section 4.

It is noted that the optimization is also an integer programming problem for variables m and n, which are integers. There are some special modifications:

(1) The initial particle should be a random integer that belongs to the feasible zone. The feasible zone is defined as $m \times n \leq Nm$, where Nm is the number of main reflector points which generate the scattering field.
(2) V_{id}^{ge+1} is a good direction for the particle, and the updated position must be integrated.
(3) The fitness is determined by the objective function which is the number of B-spline patches and it will be punished by unacceptable far field results which are compensated by the shape of the subreflector.

Specific applications are provided in Section 4.

4 CALCULATED EXAMPLES

4.1 Antenna Configuration and Distortion

The following example demonstrates the effectiveness of the method to recover the far field pattern for an antenna through subreflector shaping. A finite element method (FEM) model of a 22-m Cassegrain telescope is built which adopts an umbrella-type design to support the back of the structure, like what is used in the 100-m Effelsberg radio telescope. The primary reflector is divided into five rings and is made up of 96 panels. The back of the supporting structure for the main reflector is illustrated in Figure 3, and the parameters of the antenna are listed in Table 1.

Table 1 Geometrical Parameters of the 22-m Antenna

Main Reflector	
Reflector diameter	$D = 22\,\mathrm{m}$
Focal length/Diameter	$F/D\ = 0.33$
Offset height	$H = 0$
Tilt between axis	$\alpha = 0°$
Subreflector	
Major axis	$a = 2.97\,\mathrm{m}$
Minor axis	$b = 2.087\,\mathrm{m}$
Eccentricity	$e = 11/9$
Focal length	$f = 3.63\,\mathrm{m}$
Offset height	$h = 0\,\mathrm{m}$

Homological design has been used in structure optimization (Levy 1996) where the best fitting method is applied to eliminate structural deformities which have no adverse effects in microwave. In order to make the simulation close to reality, virtual random errors associated with the panel installation are considered and they obey a normal distribution where the mean is zero and the variance is 1/20 of the optimized structural root mean square (RMS). In addition, the polarization direction of the feed is along the x axis, and its pattern is described by

$$f_E\left(\theta'\right) = f_H\left(\theta'\right) = M\left(1 + \cos\theta'\right)\,, \tag{30}$$

where M is the magnification factor and is set to 1, and $f_E\left(\theta'\right)$ and $f_H\left(\theta'\right)$ are the patterns on the face of $\phi' = 0°$ and $\phi' = 90°$ respectively. The antenna is expected to work at 100 GHz and the primary surface is distributed into 27 094 triangular subdomains with 15 612 discrete points.

At a $45°$ angle, distortions in the main reflector cause errors in the aperture path length. This is depicted in Figure 4 where (a) and (b) are the best fitting before and after respectively (Levy 1996), and the final best fitting RMS is 0.6023 mm. The $\Delta z''_m$ of the main surface distortions are all suitable for Equation (20) which can be directly correctable without problems by the proposed approach. The antenna works at an angle and the far field pattern is not satisfactory (see Fig. 5). The deformation of the shaped subreflector can be obtained by the method described in Section 3 to compensate for distortions in the main reflector to obtain acceptable performance.

4.2 Shaped Subreflector with Zernike Polynomials

Taking the best fitting paraboloid as the theoretical reflector surface, the theoretical and real normalized patterns are shown in Figure 5. As mentioned above, several expansion functions, especially the Zernike polynomials, are evaluated, because terms in the Zernike polynomials have special geometric meaning and are widely used in optical instruments (Doyle et al. 2002). Zernike functions, in theory, are part of an infinite number of polynomials which form complete, orthogonal basis functions over the unit circle. The expression is

$$\begin{Bmatrix} Z_n^m\left(r,\theta\right) \\ Z_n^{-m}\left(r,\theta\right) \end{Bmatrix} = R_n^m\left(r\right)\begin{Bmatrix} \sin\left(m\theta\right) \\ \cos\left(m\theta\right) \end{Bmatrix}\,, \tag{31}$$

where

$$R_n^m\left(r\right) = \sum_{k=0}^{\frac{n-m}{2}} \left(-1\right)^k \frac{\left(n-k\right)!}{k!\left(\frac{n+m}{2}-k\right)!\left(\frac{n-m}{2}-k\right)!} r^{n-2k}$$
$$n = 0, 1, 2, \ldots, \left(n-m\right)\ \text{even}\,. \tag{32}$$

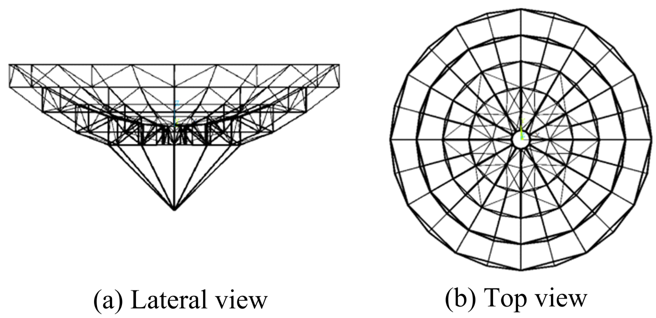

Fig. 3 The main part of the back of the supporting structure for the 22-m antenna.

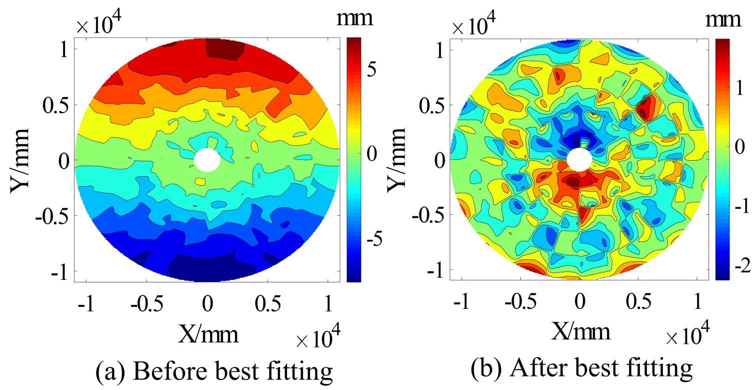

Fig. 4 The aperture pathlength error of the main reflector distortion. (The area of the inner circle is blocked by the subreflector.)

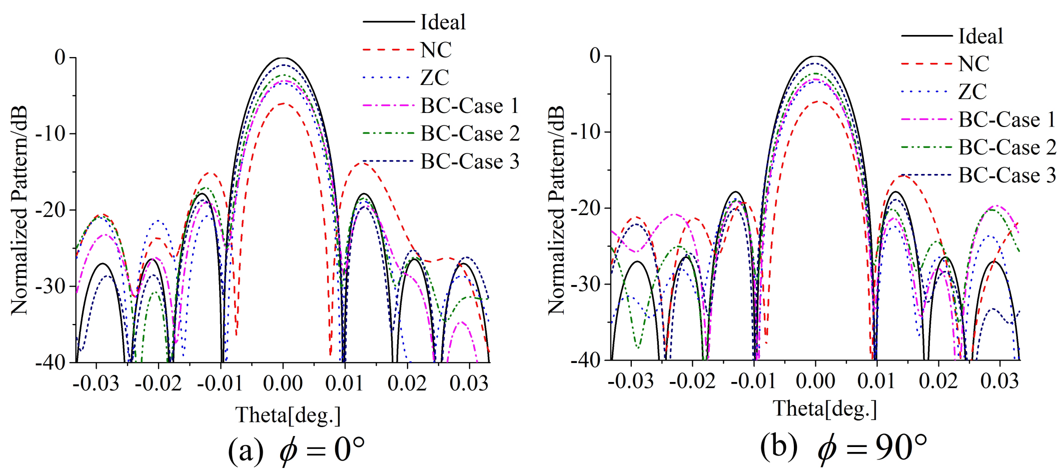

Fig. 5 The normalized pattern for the farfield at 100 GHz. (NC: No compensation for the subreflector, ZC: Zernike polynomials describing the shape of the subreflector to realize compensation, BC: B-spline surface describing the shape of the subreflector to realize compensation.)

Error in the reflectors can be expressed by a series of coefficients associated with the dominant Zernike modes as

$$f(r,\theta) = \sum_{n=0}^{\infty} \sum_{m=-n}^{n} c_{nm} Z_n^m (r,\theta) \tag{33}$$

and the coefficients can be calculated by

$$c_{nm} = \iint f(r,\theta) Z_n^m (r,\theta) \, r dr d\theta \,. \tag{34}$$

However, the global surface expressions need fast convergence and can be readily used as a synthesis tool with optimization techniques, so that the expressions

Table 2 Parameter Settings for PSO (I)

Parameter		Value
c_1		1.49
c_2		1.49
$[V_{\min}, V_{\max}]$		[–4, 4]
$[X_{\min}, X_{\max}]$		[2,200]
Population size		10
Max Iterations		300
ΔG_{Max}	Case 1	3 dB
	Case 2	2 dB
	Case 3	1 dB
$\Delta SLL_{L\_\text{Max}}$ = $\Delta SLL_{R\_\text{Max}}$	Case 1	6 dB
	Case 2	4 dB
	Case 3	2 dB

cannot be expressed by infinite polynomials, and have a small number of expected terms. The residual error of the aperture path length, which is compensated by the shape of the subreflector described by 37 terms of the former Zernike polynomials, is shown in Figure 6(a), but the results of the normalized pattern are still unsatisfactory (see Fig. 5 and Table 2). This indicates that the local characteristics of the large antenna surface, which is composed of many panels, are difficult to represent by Zernike polynomials, and the results are also suitable for other global expressions.

4.3 Shape of the Subreflector with B-spline Surface

The method that applies a B-spline surface obtains good results (see Fig. 5 and Fig. 6 (b), (c) and (d)). As mentioned in the above sections, the subreflector is shaped by the GO method and the optimal number of data points is determined by PSO so that the deformations in shape are described by the B-spline surface. To obtain an acceptable pattern for the far field, an optimal model is necessary

$$\begin{aligned} &\text{Find}: X = [X_m, X_n]^{\mathrm{T}} \\ &\text{Min}: N_{\text{patches}} = (X_m - 1) \times X_n \\ &\quad s.t.\ \Delta G \le \Delta G_{\text{Max}} \\ &\qquad |\Delta SLL_L| \le \Delta SLL_{L\_\text{Max}} \\ &\qquad |\Delta SLL_R| \le \Delta SLL_{R\_\text{Max}} \\ &\qquad (X_m \cdot X_n) \le N_{\text{main}}\,, \end{aligned} \tag{35}$$

where X_m and X_n are the number of data points in the radial and circular directions respectively, N_{patches} is the number of B-spline patches and N_{main} represents discrete points on the main reflector obtained from FEA which are regarded as precise data. The constraint, that is expected to get an acceptable far field pattern, is simplified as ΔG, ΔSLL_L and ΔSLL_R which are the reductions of gain and variation of the left and right first sidelobes respectively.

The optimization of PSO is mentioned in Section 4. To get reasonable results as soon as possible, the parameter settings and optimization process are shown in Table 2 and Figure 7, respectively.

There are three cases for the shaped subreflector which are described by the B-spline surface, and they are different from each other in terms of constraints on ΔG_{Max}, $\Delta SLL_{L\_\text{Max}}$ and $\Delta SLL_{R\_\text{Max}}$. The renormalized pattern is more satisfactory than the shaped subreflector surface which is described by Zernike functions (see Fig. 5), which can be explained in that the residual error of the aperture path length is smaller (see Fig. 6 and Table 3). The specific data are shown in Table 3, and the number of data points for the three cases of B-spline surfaces is all far less than that of Zernike functions. The good results indicate that the B-spline surface is a simple and effective way to describe the shape of the surface. It is noted that the average fitness does not need to be shown and the final results of the example may not be the globally best solution, but the results are also satisfactory and demonstrate the effectiveness of the method. In addition, the method can use a minimum number of B-spline patches to recover the required performance of the antennas, thus reducing difficulties in subreflector manufacturing. Moreover, it is also easy to add constraints related to the manufacturing ability and cost according to practical situations using the proposed method.

5 CONCLUSIONS

This paper presents a simple and useful method for shaping the subreflector surface to compensate for deterioration in the pattern of a large Cassegrain antenna. It simplifies the GO analysis by the concept of equivalent prime-focus paraboloid, and deformations of the shaped subreflector are determined by the relationship between subreflector surface distortions and the far field pattern, because the distortions in the subreflector surface will change the phase of the main surface current. It does not include any complicated iterative computations. As the surface of a large antenna is composed of many panels, there are local characteristics of the panels in addition to aberration of the entire reflector surface. The global surface expansion with orthogonal polynomials, such as Zernike polynomials, are not effective for describing it with a small number of coefficients. A B-spline surface is a simple and effective method to represent deformations in shape of the subreflector surface, which can not only provide analytical smoothing through the second derivatives, but can also represent local characteristics of the

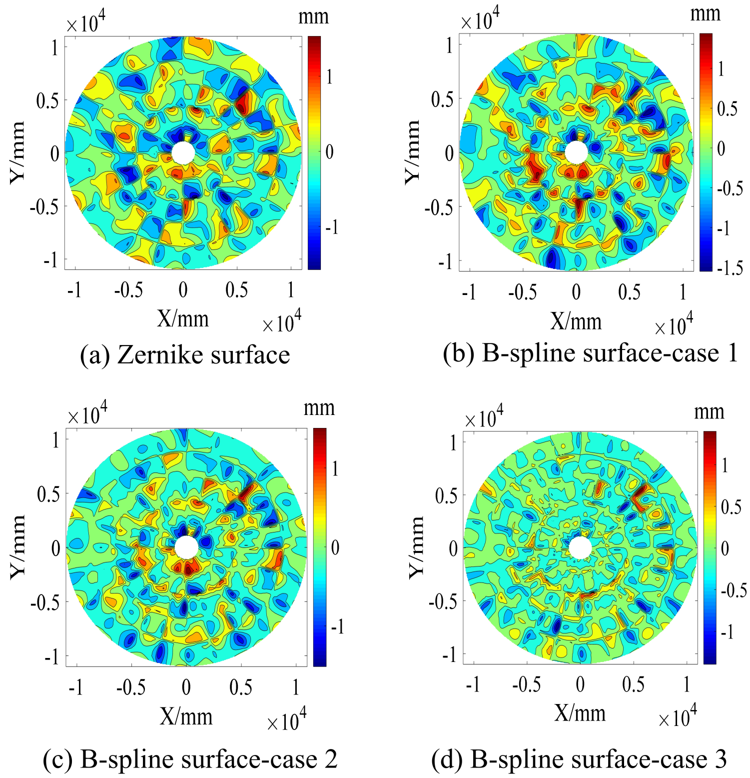

Fig. 6 The residual aperture path length error after compensation by the shaped subreflector surface.

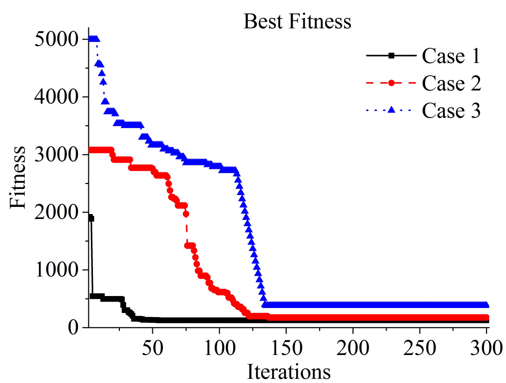

Fig. 7 The optimization process of the PSO.

surface, and can be readily used as a synthesis tool with optimization techniques. There is a complex nonlinear relationship between the number of B-spline patches and the far field pattern of the antenna, and PSO provides a good solution to search for the global optimal solution with the least number of patches for minimum manufacturing cost. A 22-m Cassegrain antenna has been presented and the results of compensation by the shaped subreflector surface are satisfactory, demonstrating the excellent performance of the proposed approach.

It is noted that the processing method described in this paper is also suitable for other types of dual-reflector antennas because the B-spline surface and PSO are universal. The difference is in the simple formulas for the relationship between deformations of the sub-reflector surface and the far field pattern, but it can be derived in the same way. In addition, the equivalent prime-focus paraboloid concept just applies to Cassegrain and Gregorian antennas. This method also provides an approach to upgrading currently-operating large dual-reflector antennas through shaping a new sub-reflector rather than costly rebuilding of the main reflector.

Table 3 Parameter Settings for PSO (II)

Surface expression of shaped subreflector		NC	ZC	BC		
				Case 1	Case 2	Case 3
$\Delta G/dB$	$\phi = 0°$	4.2845	3.0415	2.8059	1.9713	0.8109
	$\phi = 90°$	4.3198	3.0415	2.7860	1.9713	0.8109
$\Delta SLL_L/DB$	$\phi = 0°$	3.8117	3.0767	2.4726	1.9983	1.3136
	$\phi = 90°$	2.4802	2.6798	2.0637	0.9590	1.0959
$\Delta SLL_R/DB$	$\phi = 0°$	3.5826	2.5544	2.4053	1.1235	0.6563
	$\phi = 90°$	1.8733	2.4836	3.0283	1.5950	0.6617
Aperture pathlength error/mm		0.6023	0.4437	0.4417	0.3932	0.2852
The number of discrete points to describe the shape of the subreflector		/	15612	150	210	390

Acknowledgements This work was supported by the National 973 Program (No. 2015CB857100), the National Natural Science Foundation of China (Grant Nos. 51522507 and 51475349), Youth Science and Technology Star Project of Shaanxi Province (No. 2016KJXX-06), the Natural Science Basic Research Plan in Shaanxi Province (No. 2016JQ5072), the Fundamental Research Funds for the Central Universities and the Innovation Fund of Xidian University.

References

Ambrosini, R., Bocchinu, A., Bolli, P., et al. 2013, in Proc. Int. Conf. Electromagnetics in Advanced Applications (ICEAA), 82

Baars, J. W. M., & Krcher, H. J. 2018, in Radio Telescope Reflectors (Springer)

Chiu, S. T. 1996, Statisticalence, 11, 102

Doyle, K. B., Genberg, V. L., & Michels, G. J. 2002, Integrated Optomechanical Analysis, 58 (SPIE press)

Duan, B. Y., & Wang, C. S. 2009, IEEE Transactions on Antennas and Propagation, 57, 3409

Duan, D.-W., & Rahmat-Samii, Y. 1995, IEEE Transactions on Antennas and Propagation, 43, 27

Farin, G. 2002, Handbook of Computer Aided Geometric Design (Elsevier), 771

Gonzalez-Valdes, B., Martinez-Lorenzo, J. A., Rappaport, C., & Pino, A. G. 2013, IEEE Transactions on Antennas and Propagation, 61, 467

Hoferer, R. A., & Rahmat-Samii, Y. 2002, IEEE Transactions on Antennas and Propagation, 50, 1676

Huang, L. W., & Jin, Z. T. 1986, Reflector Antenna (Xian: Northwest Telecommunication Engineering Institute Press), in Chinese

Imbriale, W. A. 2001, in Proc. (Cat. No. 01TH8542) 2001 IEEE Aerospace, 2, 2/799

Lamb, J. W., & OVRO, C. 2001, Verification of Ruze Formulas By Comparison with Ray-Tracing

Levy, R. 1996, Structural engineering of microwave antennas for electrical, mechanical, and civil engineers (Piscataway, NJ: IEEE Press)

Prestage, R. M., Constantikes, K. T., Hunter, T. R., et al. 2009, IEEE Proceedings, 97, 1382

Rahmat-Samii, Y. 1984, IEEE Transactions on Antennas and Propagation, 32, 301

Rahmat-Samii, Y. 1991, IEEE Aerospace Electronic Systems Magazine, 6, 12

Robinson, J., & Rahmat-Samii, Y. 2004, IEEE Transactions on Antennas and Propagation, 52, 397

Ruze, J. 1966, IEEE Proceedings, 54, 633

Ruze, J. 1969, Small Displacements in Parabolic Reflectors, Lincoln Laboratory Memorandum

Silver, S. 1949, Microwave antenna theory and design (McGraw-Hill Book Co), 267

Smith, W. T., & Bastian, R. J. 1997, IEEE Transactions on Antennas and Propagation, 45, 5

von Hoerner, S. 1976, IEEE Transactions on Antennas and Propagation, 24, 336

von Hoerner, S., & Wong, W.-Y. 1979, IEEE Transactions on Antennas and Propagation, 27, 720

Wielebinski, R., Junkes, N., & Grahl, B. H. 2011, Journal of Astronomical History and Heritage, 14, 3

Xu, Q., & Wang, N. 2016, in Ground-based and Airborne Telescopes VI, 9906, International Society for Optics and Photonics, 99065L

Xu, S., Rahmat-Samii, Y., & Imbriale, W. A. 2009, IEEE Transactions on Antennas and Propagation, 57, 364

Zarghamee, M. S. 1982, IEEE Transactions on Antennas and Propagation, 30, 1228

Zarghamee, M. S., Antebi, J., & Kan, F. W. 1995, IEEE Transactions on Antennas and Propagation, 43, 79